A unique Tandem RAman Microscopy (TRAM) integrating spontaneous and coherent Raman scattering offers integrated data analysis to improve optical biosensing

K. Brzozowski[1], A. Pieczara[2,3], W. Korona[1,2], A. Nowakowska[1], B. Orzechowska[1], J. Firlej[1], A. Wislocka-Orlowska[1], M. Baranska[1,3,*]

[1]Jagiellonian University, Faculty of Chemistry, Gronostajowa 2, 30-387, Krakow, Poland
[2]Jagiellonian University in Kraków, Doctoral School of Exact and Natural Sciences, 11 Lojasiewicza St., Krakow, Poland
[3]Jagiellonian University, Jagiellonian Centre for Experimental Therapeutics (JCET), Bobrzynskiego 14, 30-348 Krakow, Poland

Correspondence to: Malgorzata Baranska, m.baranska@uj.edu.pl

Abstract
For the first time, we provide Tandem RAman Microscopy (TRAM), a cutting-edge multimodal microscope that integrates the methods of Stimulated Raman Scattering (SRS), Coherent anti-Stokes Raman Scattering (CARS), and spontaneous (resonance) Raman Scattering ((R)RS). The device facilitates sequential RS imaging to collect full spectra from every sample location and rapid SRS-CARS scanning at specific wavelengths, offering a reliable and efficient analytical tool. The fingerprint spectral region can be included in the spectral imaging capabilities of CARS and SRS. Additionally, the flexibility of measuring conditions is improved by offering resonance-enhanced RS measurements using a continuous wave (CW) laser with two scanning mode options (high-speed galvo-scanners and a piezo-driven precision translation stage). We analyze the *in vitro* model of nonadherent leukocytes to illustrate the capabilities of this unique system, emphasizing the benefits of measuring the same sample with three different techniques without having to transfer it between microscopes. Additionally, polystyrene was investigated as a non-biological material. The advantages of each Raman technique are utilized when (R)RS, SRS, and CARS are combined into a single device. This paves the way for dependable chemical characterization in a wide range of scientific and industrial fields.

Keywords:

Raman microscopy, resonance Raman scattering, stimulated Raman scattering, coherent anti-Stokes Raman scattering, CARS-SRS-RS, multimodal imaging, nonlinear optics, leukocytes, polystyrene

Introduction
Understanding a material's structure and composition is essential to deciphering the language of nature and comprehending its behaviours, properties, and functions. However, because of the intrinsic intricacy of the issue and the limitations of individual analytical tools, getting such information might be difficult.
An analytical method needs to meet several criteria to be deemed reliable, and measurement requirements include: (i) high accuracy and precision, (ii) high selectivity and sensitivity, (iii) assessment of both qualitative and quantitative properties, (iv) versatility enabling application to a variety of sample types, (v) minimal sample preparation and non-destructiveness, (vi) high speed and high throughput, (vii) robust performance, (viii) easy to use, cost-effective, portable, and compatible with various experimental conditions, and, most importantly, (ix) offering high spatial resolution imaging capabilities[1–5].

The majority of these requirements are met by spectroscopic techniques, including Raman microscopy, and, therefore, they are widely used in many fields as tools to assess chemical and structural information even from fragile samples.
Raman spectroscopy is a fundamental analytical method in the field of material sciences and biology, offering non-invasive probing of the molecular composition of samples. It is based on Raman effect [1], a phenomenon in which incident light is inelastically scattered by a sample. The so-called Raman shift provides information about the molecular vibrational energy of sample components, which allows for their detailed chemical analysis.
Among Raman techniques, spontaneous Raman scattering spectroscopy (RS) is the most widely used, which records a linear response of a sample to the applied electric field. Various applications of RS in chemistry [2], materials science [3], biology [4], and medicine [5] are focused on the identification and quantification of substances, the study of molecular interactions, and the monitoring of biochemical changes in live cells. Despite the universality and comprehensiveness of the RS technique, it has some limitations, particularly in terms of speed and sensitivity [6], which is an obstacle when dealing with biological samples that may be susceptible to damage under prolonged exposure to highly focused laser light. Sensitivity can be significantly enhanced by measuring the electronic transition, as is the case for resonance RS (RRS). Regarding speed, data acquisition in RS is conducted using translation stages equipped with piezo-elements, which provide high accuracy down to fractions of a micrometer. Although this process is relatively slow, the scanning speed of the translation stage nonetheless exceeds the time required for the stage to capture the Raman spectrum at a given measurement point. In most instances, there is no necessity for employing faster scanners in RS – the speed limitations inherent to RS stem from its linear nature and the weak signals involved, necessitating longer exposure times at each measurement point. Moreover, a major problem for RS is fluorescence, which often obscures the Raman signal, making molecular composition detection difficult [7].
Coherent anti-Stokes Raman Scattering (CARS) and Stimulated Raman Scattering (SRS) overcome the intrinsic challenges encountered in RS by providing enhanced signal strength and rapid measurements. Both techniques pioneered Coherent Raman Scattering (CRS) methods since their invention revolutionized the way of vibrational imaging with a video-rate timescale[8,9]. For example, in the case of biological material, the RS signal for a single pixel is collected in several hundred milliseconds, whereas detection of the CARS or SRS signal takes tens of microseconds. Therefore, in imaging using nonlinear optics techniques, where information about one component is obtained at the expense of the entire Raman spectrum, the measurement time is several orders of magnitude shorter than in the case of RS[6]. That is achieved by employing galvo-scanners, which enable measurements by the movement of a laser beam as an alternative to piezo stage scanning[7].

The fundamentals of CARS are based on a four-wave mixing process encompassed by joint interaction between coherently incident Stokes and pump photons with the sample to generate a new field at anti-Stokes frequency[10]. Current applications of CARS exhibit growing interest in the field of biomedical samples endoscopy[11] and intracellular metabolism[8,12] while offering an enhanced Raman signal with an increased selectivity of imaged molecule vibrations. The capability of tuning the pump and Stokes frequency difference in CARS to match the symmetric stretch vibrations of the CH_2 groups showing a large Raman scattering cross section has been demonstrated in multiple studies on lipid metabolism in cells[24], tissues[25], and model organisms[26]. Despite multiple advantages, the CARS signal suffers from the contribution of a non-resonant background, requiring the application of e.g. phase retrieval algorithms to obtain valuable information[8,9].

Similarly to CARS, SRS spectroscopy is based on the 3rd order nonlinear effect that enhances the Raman signal through the interaction of the sample with a pump beam and a Stokes beam. Compared to CARS, SRS's imaging capabilities based on rapid galvo-scanners and picosecond lasers, enable ultrafast imaging of specific Raman bands and better discrimination against non-resonant background [13]. SRS has proven to be particularly beneficial for biological applications, as high-throughput measurements allow capturing dynamic processes [13] and minimizing damage [14] to the sample.

Using CARS and SRS imaging, two nonlinear optics techniques that have a distinct physical origin than RS phenomena, offers benefits and therefore provides a more comprehensive insight into the vibrational state of samples [15]. However, despite the advantages of CARS and SRS over RS, there are a few challenges and considerations with CRS techniques that need to be taken into account. The undeniable advantage of CRS is its high confocality and the possibility to register a discrete signal that comes only from the vibration of a certain energy. On the other hand, analysis based solely on a single selected signal may be difficult when the energy of vibrations from various molecules is similar and their Raman bands overlap. The reliable Raman microscope should therefore combine the advantages of the speed and efficiency of nonlinear optics spectroscopic techniques with the robustness of spectroscopic interpretation through the analysis of the Raman spectrum obtained with RS. Therefore, we propose the Tandem RAman Microscope (TRAM), which integrates the best of Raman scattering techniques, i.e. (R)RS, CARS, and SR, into a single platform.

Because CARS and SRS signals are generated simultaneously at different wavelengths when the sample is illuminated with pump and Stokes beams, it is possible to detect both CARS and SRS using one microscope[10]. This approach was applied effectively for studying the dynamics of biological systems[28,29].

Some attempts have already been made to combine CARS or/and SRS with RS. The combination of CARS and RS was used for a quantitative analysis of lipid bodies [27], and revealed differences in the level of unsaturation and the abundance of exogenous fatty acids in the adipocytes. Both CARS and RS measurements were performed on the same platform with the use of a picosecond laser and galvo-scanner. This approach was further enriched by independently conducting lipid droplet analyses through SRS and RS, however on distinct samples separate from those for CARS and RS. That experimental setup offered the capability for simultaneous RS, SRS, and CARS measurements, however with certain constraints, primarily the use of a picosecond instead of CW laser with no flexibility for choosing a UV-VIS laser source for RS excitation, especially useful for RRS. A combined analysis using SRS and RS imaging has also been demonstrated, e.g. to distinguish normal tissue from cancerous tissue in mouse fibrosarcoma[16]. RS showed the potential of enhanced accuracy diagnostics for future spectral histopathology. Both imaging techniques were also used to study the distribution of lipids in the skin[17]. The combined analysis helped to reduce the dominant protein background and cross-sensitivity for blended Raman bands allowing the extraction of spectra of skin lipids. In the pharmaceutical area, integration of SRS and RS was used to follow the spatial distribution of amlodipine besylate in tablets, which is a commonly used blood pressure-lowering drug[18]. Both techniques have been applied to the cancer detection and drug development process[19]. However, in this case, SRS and RS measurements were performed using separate microscopes, so it was difficult to maintain the same conditions and measurement area.

RS and SRS analysis also have the potential for real-time monitoring of dynamic processes. The capability of SRS to capture dynamic changes in molecular composition has already been demonstrated in the progression of degenerative diseases, such as atherosclerosis[20] or lipogenesis[21]. Moreover, imaging sensitivity and selectivity can be further enhanced by labelling, i.e. by utilizing specific Raman reporters containing an isotopic or alkyne tag [20]. In a study of atherosclerosis, Stiebing et al. showed repeated measurements of the same cells over

time to track metabolic processes in real-time using both SRS and RS, but separately. They showed how important it is for capturing cell-to-cell variability to track changes over time in the same cells, rather than taking measurements at different time points of different cellular populations at corresponding intervals [20]. The ability to measure the same cells over time and with different techniques is therefore crucial to fully understand the complexity of the systems under study, as well as to fully correlate the information obtained by different methods and minimize the impact of cell mobility and the need for spatial calibration. The complementarity of RS and SRS measurements is also used for material characterization and design, allowing *in situ* studies on dynamic processes, e.g. ion transport [22] or polymerization [23].
Despite previous efforts, no technological solution has been presented that combines three Raman modalities in one device, i.e. (R)RS, SRS, and CARS, especially with the possibility of using a CW UV-VIS laser enabling flexible measurement of (R)RS.
Here we demonstrate TRAM, a tandem system using linear optic (RS) and two nonlinear Raman techniques (CARS and SRS) integrated in a single platform for both spectral characterization and imaging. On the one hand, TRAM provides co-located RS and CARS-SRS microscopy with hyperspectral data acquisition for greater credibility for the obtained results, and eliminating the limitations of each of Raman scattering methods when used separately. On the other hand, it yields a broader versatility and flexibility of the measurement conditions on one platform, making it relevant to a wider range of samples and research scenarios, from material sciences to biological studies. Compared with existing spectroscopic imaging systems, TRAM has several novelties, including the simultaneous integration of three different spectroscopic techniques (i.e. CARS, SRS, and RS) with microscopy, the extension of spectral imaging using CARS and SRS concurrently to the fingerprint region, and the ability to enable two modes of sample scanning, i.e. a high-speed galvo-scan and a precise piezo-driven translating stage. Innovatively, we used a CW 532 nm laser for RS acquisition, which offers very sensitive RRS measurements. For the first time, we demonstrate the application of TRAM to measure two types of samples, i.e. biological, live leukemia cells and non-biological polystyrene beads, using complementarily (R)RS, SRS, and CARS, over a wide spectral range, under the same conditions, without transfer samples.

Methods

Tandem RAman Microscopy (TRAM)

We used TRAM for in-depth spectroscopic analysis using a multimodal approach that combined RS, SRS, and CARS.
The integration of the *WITec* spectrometer (*WITec* GmbH, Germany) equipped with a CCD detector (*Andor Technology Ltd.,* Northern Ireland) and a 600 grooves/mm grating (BLZ = 500 nm) in conjunction with electronics and *Control SIX 6.1* software (*WITec* GmbH, Germany) was used for RS microscopy, together with a 532 nm continuous wave (CW) laser (*WITec* GmbH, Germany) with an average power output of 50 mW. The same electronics and software were used for SRS and CARS, which makes the system exceptionally useful.

The core of SRS and CARS setup in the TRAM is the picosecond laser system (*Fluence Lazurite*, *Fluence sp. z o.o.,* Poland). It includes a fiber-based Stokes laser that can produce an average power of 450 mW at a 1029 nm wavelength. Additionally, the system features a built-in Optical Parametric Oscillator (OPO) that generates a tunable pump beam, ranging from 750 to 950 nm, with an average power of 100 mW. Both the Stokes and pump beams produce 2 ps pulses with a 20 MHz repetition rate. To get the beams ready for nonlinear optics imaging, they are first overlapped in space using a dichroic mirror and aligned in time with an optical delay line (ODL) in the path of the pump beam. The Stokes beam is modulated at a 4 MHz frequency using an Acousto-Optic Modulator (AOM).

The beams are directed to the sample using a 2-axes piezo mirror galvo-scanner attached to a *Nikon Ti2* inverted microscope (*Nikon Corp.,* Tokyo, Japan). An *UPLXAPO40X* NA 0.95 40× *Olympus* (*Olympus Corp.,* Tokyo, Japan) air objective lens focuses the laser beams onto the sample. For signal collection, we use the same lens (RS epi-detection), and an *MRD07620* 50× NA 1.0 *Nikon* (*Nikon Corp.,* Tokyo, Japan) water dipping objective lens (SRS and CARS detection).

A *Thorlabs SM1PD1* photodiode (*Thorlabs Inc*., US), and *Stanford Research Systems SR865A* (*Stanford Research Systems*, CA, US) lock-in amplifier which demodulates the signal is used for SRS collection, while *Hamamatsu R9110* (*Hamamatsu Photonics*, Japan) photomultiplier tube plus *Stanford Research Systems SR570* (*Stanford Research Systems*, CA, US) preamplifier are used for CARS collection.

For the CARS collection, we removed unwanted non-resonant background by applying optical filters that remove Rayleigh and SHG signals. Additionally, Stokes and pump signals were carefully removed so as not to disturb the CARS signal.

Fig. 1a-b. presents TRAM setup along with energy diagrams and a comparison of the imaging methods used in TRAM.

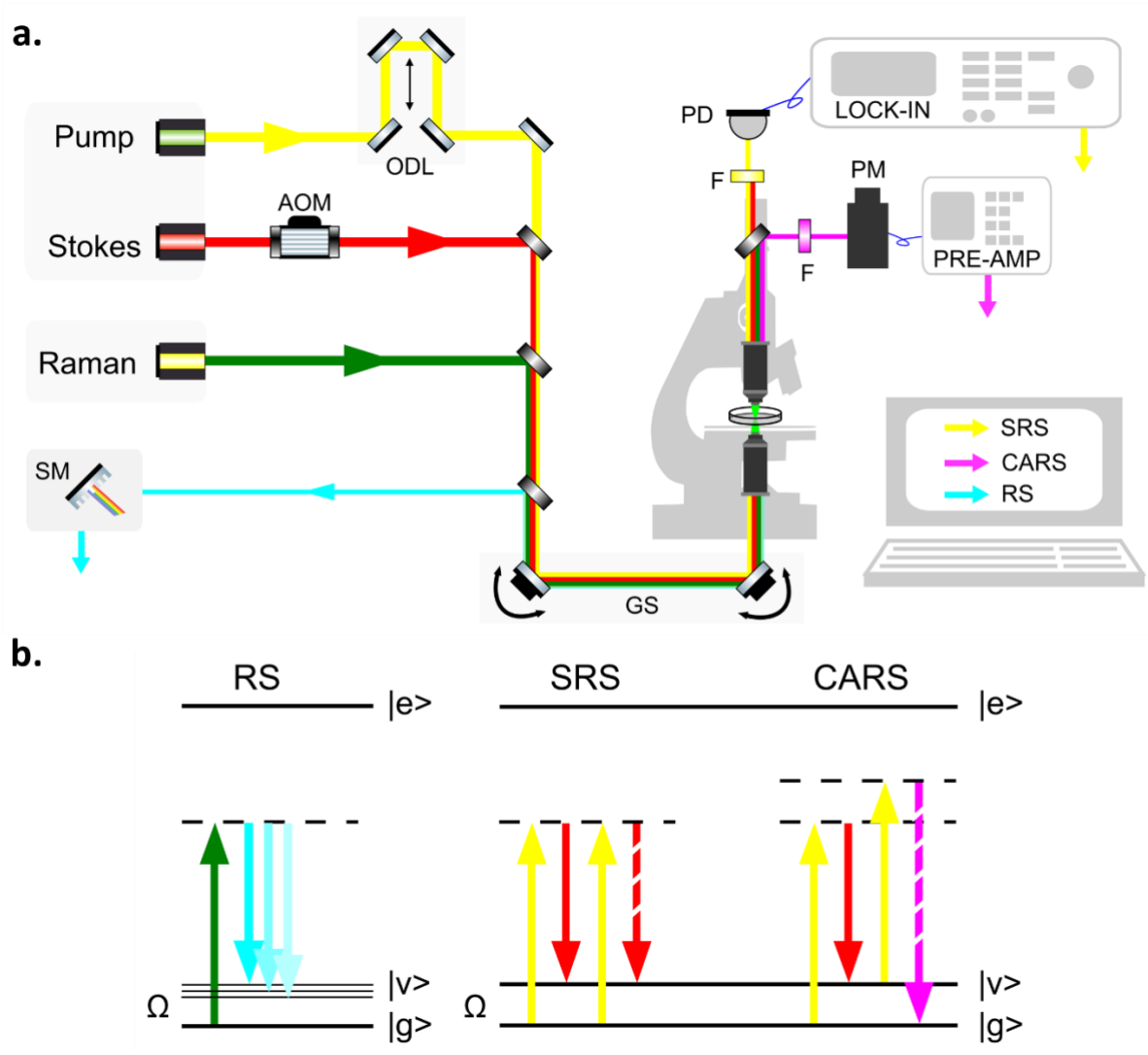

Fig. 2. ***a.*** *TRAM setup; AOM – Acousto-Optic Modulator, ODL – Optical Delay Line, F – optical filters, PD – photodiode, PM – photomultiplier tube, GS – galvo-scanner, SM - spectrometer.* ***b****. Energy-level diagrams of RS, SRS, and CARS.*

Table 1. *Methods comparison.*

Abbreviations: DT_{min} – the lowest possible pixel dwell time, $DT_{in\ use}$ – pixel dwell time typically used for measurements, D_{Abbe} – spatial resolution calculated based on the Abbe's criterion, $D_{in\ use}$ – pixel size typically used for measurements, S/N_{lipids} – a signal to noise ratio for imaging of lipids in cells, S/N_{PS} – signal to noise ratio for imaging of polystyrene beads, $Area_{max}$ – maximum area that can be scanned, $Area_{in\ use}$ – area that is typically used for measurements.

	properties	RS	SRS	CARS	TRAM
speed	speed of the measuremnts [s]	DT_{min}=0.001 $DT_{in\ use}$=0.5	$DT_{min}=10^{-5}$ $DT_{in\ use}=3\text{-}9\cdot10^{-4}$		
speed	spatial resolution [µm]	D_{Abbe}~ 0.35 $D_{in\ use}$~1	D_{Abbe}~ 0.25 $D_{in\ use}$:0.3-0.5		
speed	contrast and visualization of fine structures	S/N_{lipids}=18.72 S/N_{PS}=10.84	S/N_{lipids}=43.16 S/N_{PS}=59.43	S/N_{lipids}=30.08 S/N_{PS}=101.89	
speed	scan [µm]	Piezoelectric translative table Galvo-scaner $Area_{max}$> cm	2-axes galvo-mirrors scanner $Area_{max}$: 200x200 $Area_{in\ use}$:100x100		
spectral information	spatial interpretability [cm^{-1}]	-73.3-33758.4	1011-3615 *discrete wavenumbers	1169-3303 *discrete wavenumbers	
spectral information	spectral sensitivity				
spectral information	signal strenght proportional to molecule concentration				
interference	interference from fluorescence				
interference	interference from non-resonant background				
experimental and sample needs	solvent compatibility				
experimental and sample needs	glass substrate compability	* require objective with glass correction			
experimental and sample needs	non-label and labelled approach				
measurement parameters	excitation [nm] (possible resonance)	possible: 488, 532, 633 in use: 532	pump: 750-950 Stokes: 1029		
measurement parameters	maximum laser power on the sample [mW]	532 nm ~ 25	pump: 25 Stokes: 25		
measurement parameters	direction of detection	epi-detection/ inverted microscope	transmission/ inverted microscope		
measurement parameters	detector	sectrometer + CCD	photodiode + lock-in	photomultiplier + preamplifier	
measurement parameters	objective lens	ilumination/ colection: Olympus air UPLXAPO40X 40× NA 0.95	ilumination: Olympus air UPLXAPO40X 40× NA 0.95 collection: Nikon water deeping MRD07620 50XNA 1.0		

Experimental Parameters

RS measurements of cells were performed using TRAM set to approximately 24 mW average power of the 532 nm beam, a pixel dwell time (PDT) of 500 ms, a fixed pixel size of 1 µm x 1 µm, and a frame size of 40 µm x 40 µm. Also, polystyrene (PS) beads were examined. In the case of PS beads the power was set to approximately 12 mW, PDT of 50 ms, fixed pixel size of 1 µm x 1 µm, and a frame size of 50 µm x 60 µm.

For SRS and CARS imaging of cells, the system was configured to an average power of approx. 24 mW of the Stokes beam and approx. 12 mW of the pump beam. The SRS frames were captured with a PDT of 900 µs, a fixed pixel size of 500 nm x 500 nm, and a frame size of 40 µm x 40 µm. In the case of PS beads the power was set to approx. 6 mW of the Stokes beam and 3 mW of the pump beam, PDT of 900 µs, fixed pixel size of 500 nm x 500 nm, and a frame size of 50 µm x 60 µm.

Our TRAM setup allows for two types of scanning. Firstly, fast scanning using a piezo-driven stage is possible, which is utilized in RS measurements. Secondly, there is an option for even faster scanning using a dual-axis galvo-scanner, which was employed in SRS and CARS measurements.

Cells preparation

Human promyelocytic leukemia HL-60 (ECACC 98070106) cells were cultured in Roswell Park Memorial Institute (RPMI) 1640 medium supplemented with glutamine and 10% Fetal Bovine Serum. Cell culture was kept at 37 ^{o}C, 5% CO_2/95% in the air-humidified incubator. Cell density was maintained below one million cells per milliliter. Cells were incubated with 200 µM of palmitic acid (Sigma Aldrich) for 24h. Just before measurements, the cells were rinsed with warm PBS. For all measurements, live cells were placed onto CaF_2 slides, and suspended in a droplet. Measurements were performed after cell sedimentation and immobilization.

Image processing and software

Data from RS, SRS, and, CARS were analyzed by employing *Project FIVE 6.1 software* from *WITec*. Preprocessing of Raman spectra included Cosmic Ray Removal (CRR; filter size: 4; dynamic factor: 4) and Background Subtraction (BG; polynomial order: 3), then a KMC (*k*-means cluster) analysis was performed. Both measurements and data analysis were operated by one software, which is intuitive and makes work significantly easier. Origin 2021 (OriginLab Corporation) was used for data presentation.

Results

We demonstrate the versatility of the TRAM setup by examining its applications in the fields of biological and materials sciences. Biological research employing spectroscopic techniques is increasingly used to solve various biological problems involving single molecules, cell components, organelle activity, and more complex whole metabolism of the cell. This field of science is rapidly developing; therefore, it is important to simplify and speed up measurements by employing different techniques for analysis at the same time. Materials science is a diverse and interdisciplinary field that focuses on creating and finding new solid materials, including metals, polymers, semiconductors, and ceramics. Research in this discipline focuses on analyzing the correlation between a material's structure, qualities, and manufacturing process. Spectroscopy has also found its niche in this field showing the use of SRS[11–14] and CARS[15–17] for testing different properties of materials.

TRAM in biological science

We successfully employed TRAM to assess the metabolic state of live leukemia cells using three spectroscopic modalities, RS, SRS, and CARS, over a wide spectral range, also in the fingerprint range, all under the same conditions (**Fig. 2a-c**) . The advantage of TRAM in that is no need to transfer the sample from one microscope to another is particularly important in the case of non-adherent cells such as leukemic cells. RS was used here to register full spectra and select of bands for further SRS and CARS measurements. SRS and CARS images (

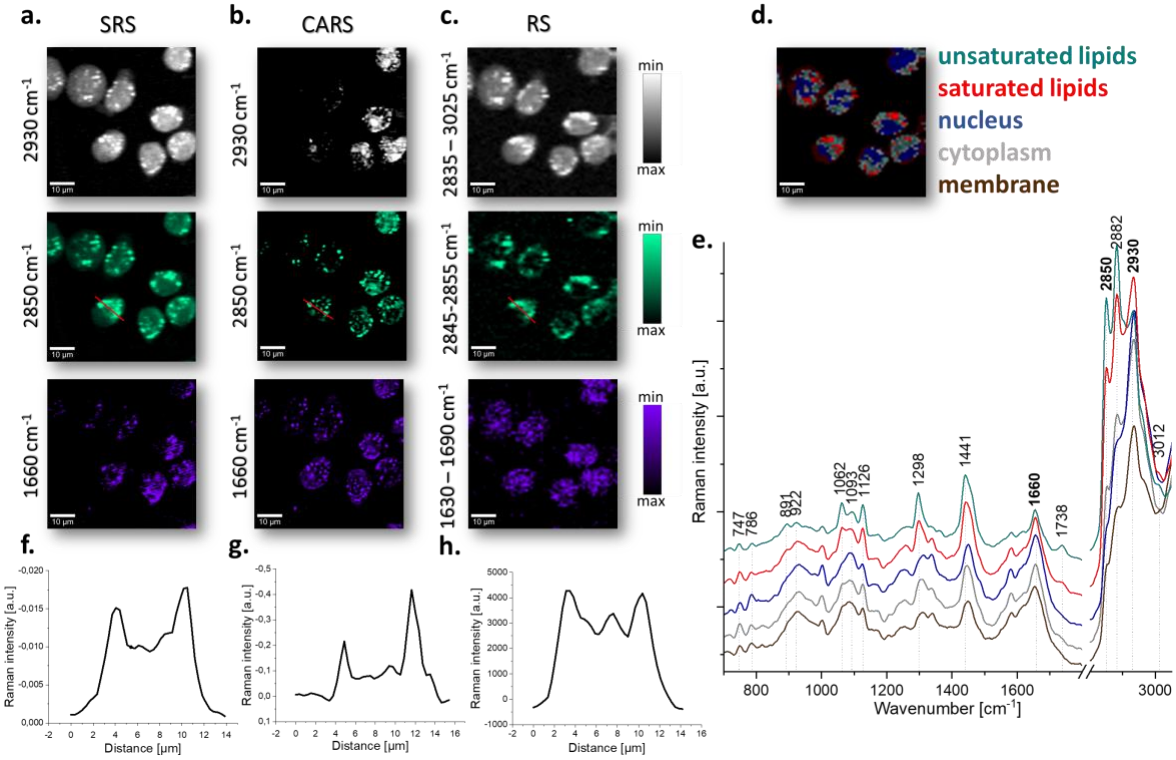

Fig. 3a-b) were collected using a pump beam at 791 nm (2930 cm^{-1}), mainly corresponding to proteins and showing cell morphology, 795 nm (2850 cm^{-1}), mainly corresponding to lipids, and 879 nm (1660 cm^{-1}), corresponding to lipids and proteins. RS images (

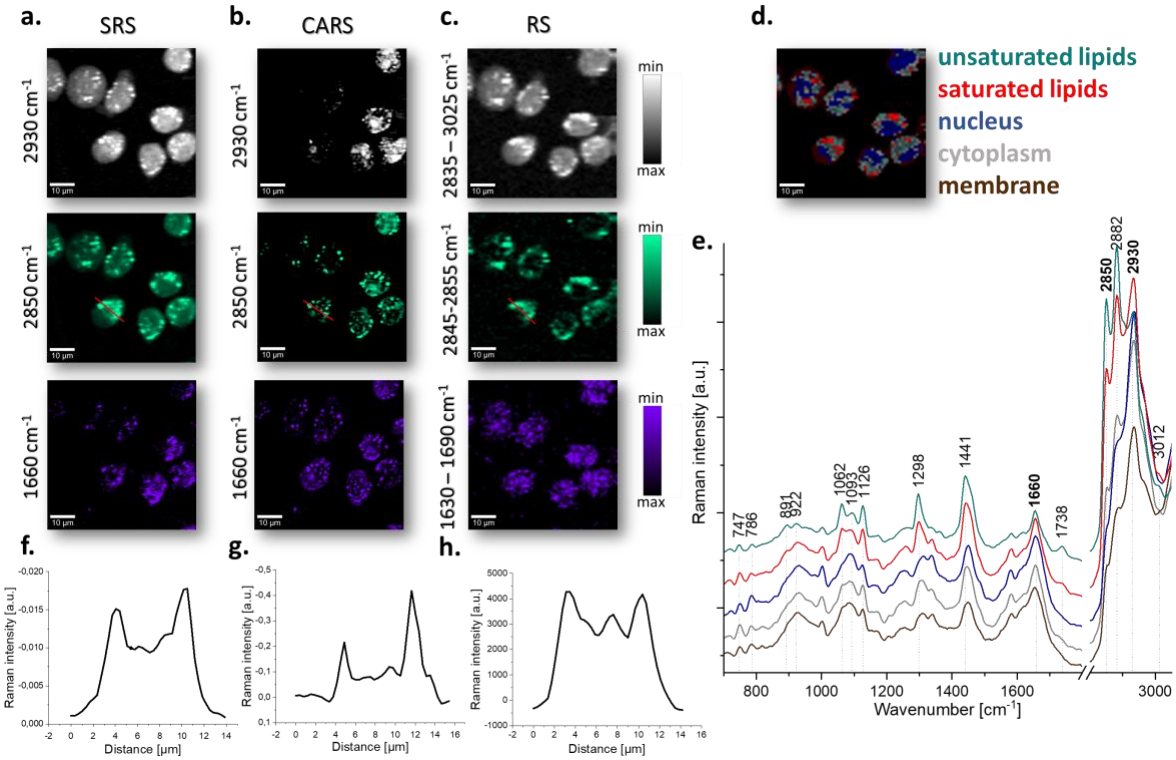

Fig. 3c) were obtained by integrating the characteristic Raman bands and provide information about the composition of the cell (2835-3025 cm^{-1}, CH stretching), the subcellular localization of endogenous lipids (2845–2855 cm^{-1}, ν(CH) in CH_2 stretch), and the subcellular localization of lipids and proteins (1630-1690 cm^{-1}, ν(C=C) stretching, amide I). Moreover, the *k*-mean cluster (KMC) analysis showed the spatial distribution of the cellular components (

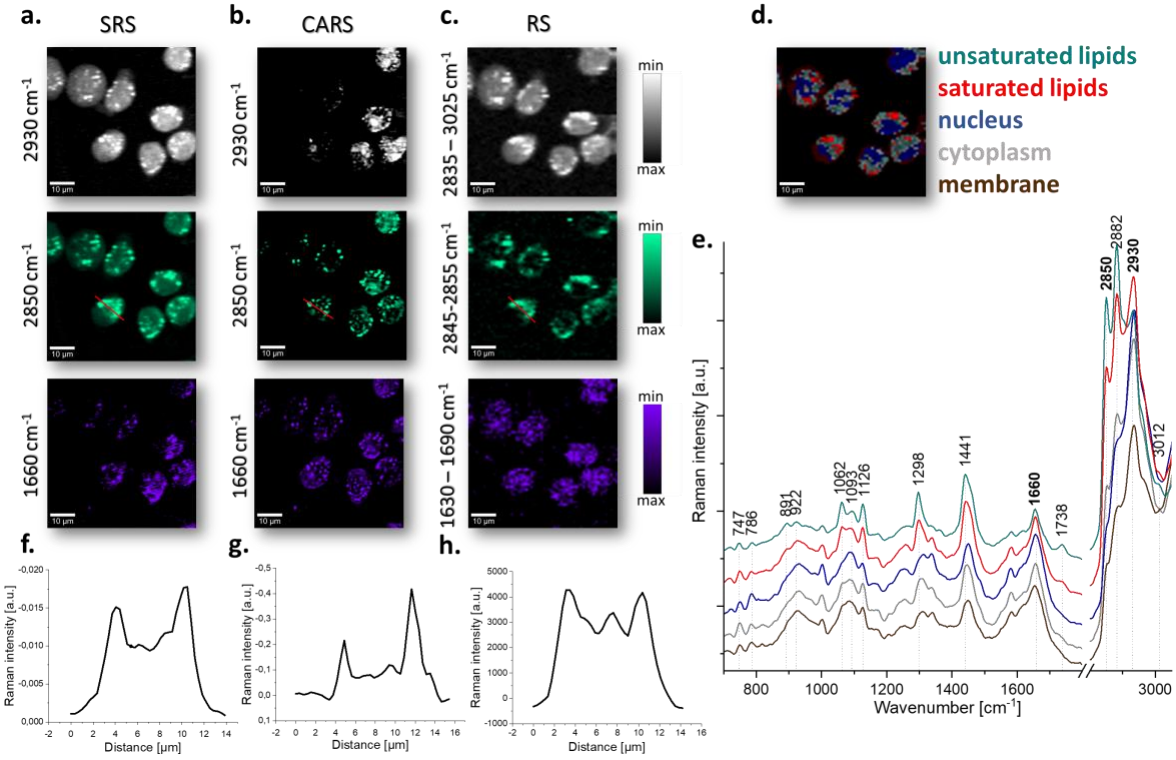

Fig. *3*d). The mean spectra of unsaturated lipids, saturated lipids, nucleus, cytoplasm, and membrane are presented in

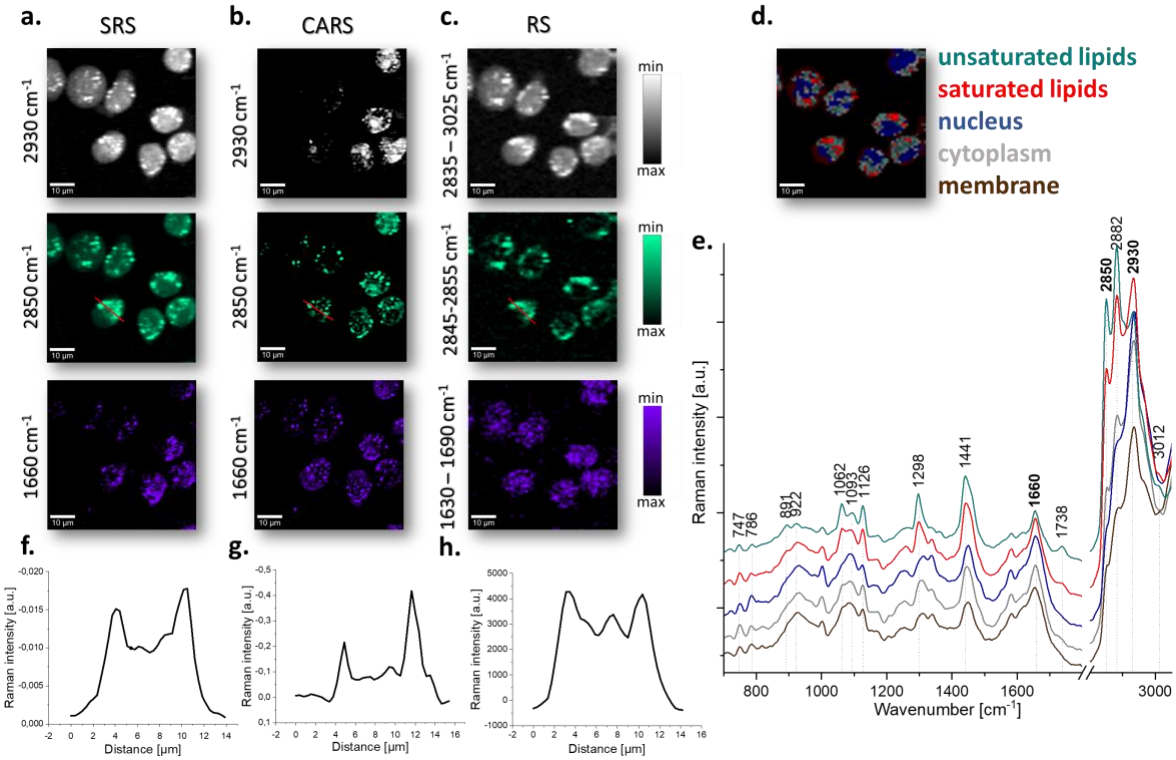

Fig. *3*e.

A strong correlation is observed between the SRS and RS images that depict lipid morphology. The discrepancy between the SRS and CARS images, notably at 2930 cm^{-1}, is attributed to the variation in the focal planes of cells across different frame locations combined with a weaker CARS signal.

Distinguishing differences between SRS, CARS, and, RS images regarding signal become apparent when examining lipid distribution at 2850 cm^{-1}. This disparity arises from the relatively broad integration range employed to visualize the heterogeneous lipid fraction in RS (10 cm^{-1}), juxtaposed with the discrete, specific wavenumber value chosen for the SRS and CARS measurements.

The measurement time for RS and CRS was significantly different, i.e. imaging of cells using the RS took several minutes (~ 25 min), while the SRS and CARS images were obtained in a few seconds (14 s), although the step size was twice as small for SRS and CARS (0.5 µm) in comparison to RS (1 µm). This shows the advantage of CRS imaging in terms of speed.

The SRS images are sharp and the contrast between the signal and the background is high. As presented in

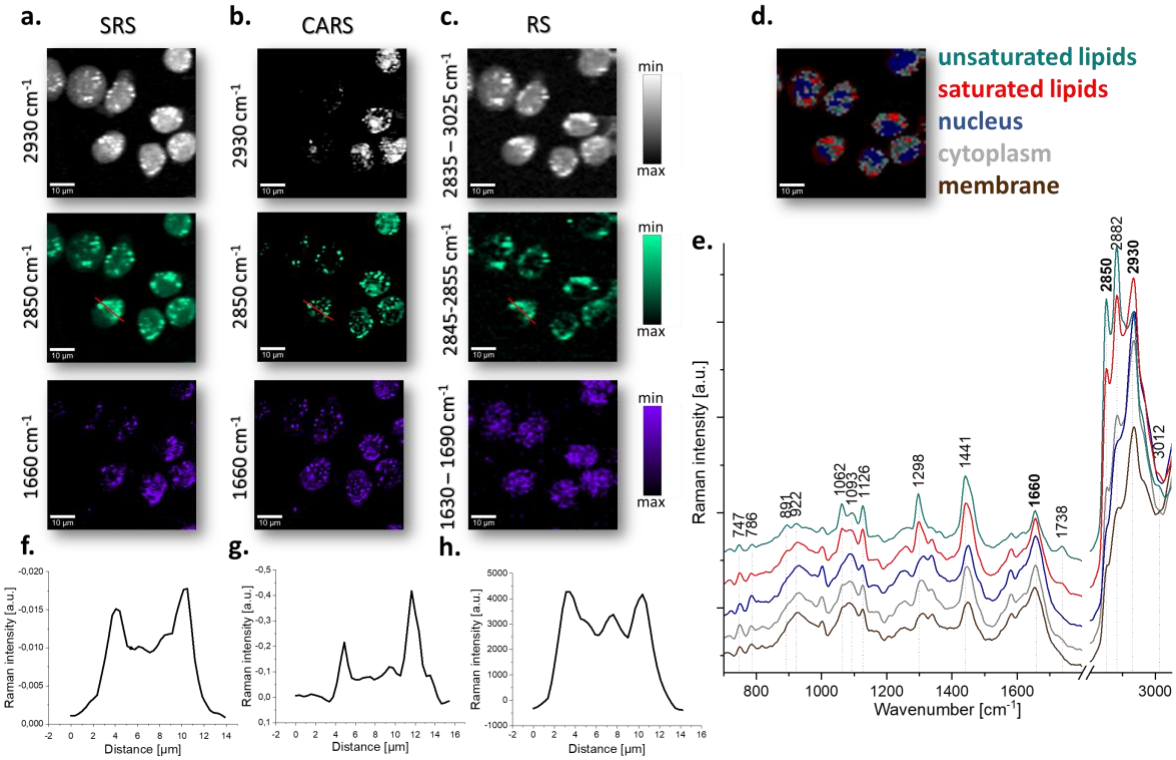

Fig. *3*f-h, the signal-to-noise ratio (S/N) calculated along the cross section in images showing the distribution of lipids is around two and half times higher for SRS images (43.16) and about two times higher for CARS images (30.08) in comparison to the corresponding RS images (18.72). The SRS signal does not suffer from a non-resonant background, which greatly improves the quality of the SRS images and lowers the noise. Additionally, the measurement step size is two times smaller for SRS and CARS than for RS, ensuring better visualization of details in the cell structure for the first approach, e.g. the perinuclear area was visualized distinctly using the SRS technique.

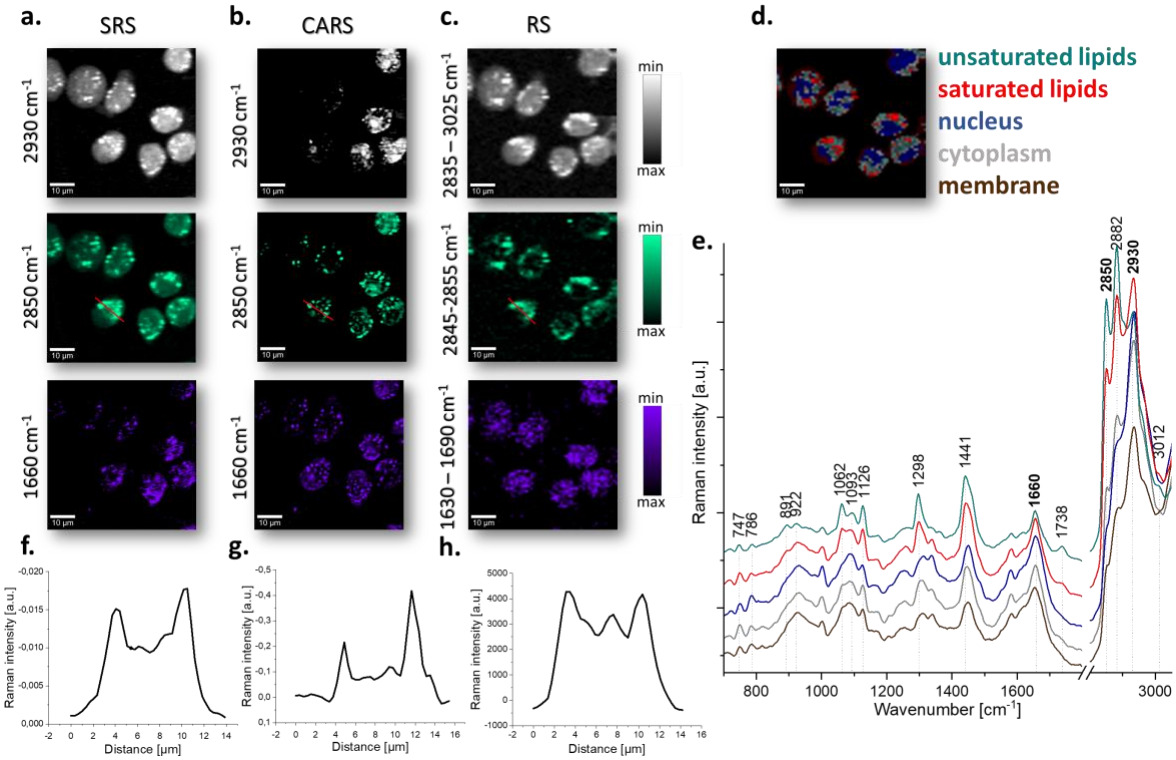

***Fig. 3. SRS/CARS/RS images of live HL-60 cells**. **a**. - **b.** SRS and CARS images were collected using a pump beam of 791 nm (2930 cm^{-1}, organic matter), 795 nm (2850 cm^{-1}, lipids), and 879 nm (1660 cm^{-1}, lipids and proteins) respectively. **c**. Representative RS images were obtained by the integration of the selected Raman bands at 2835-3025 cm^{-1} (organic matter), 2845-2855 cm^{-1} (lipids), and 1630-1690 cm^{-1} (lipids and proteins), respectively. **d**. KMC map, showing the distribution of cell components in HL-60 cells. **e.** The averaged Raman spectra of cell components: unsaturated lipids (green), saturated lipids (red), nucleus (blue), cytoplasm (grey), and membrane (brown). **f-h**. Intensity profiles of Raman signals collected along the cross-section (highlighted in red) in images showing the distribution of lipids obtained using SRS, CARS, and RS, respectively. Scale bar: 10µm. SRS and RS scans were performed respectively using a galvo-scanner and a translation table.*

Resonance-enhanced RS is a very unique approach that enables the detection of a specific group of chemical components. To meet the requirements to obtain RRS it is necessary to adjust the energy of the excitation wavelength to the electronic transitions of the molecule[18]. In TRAM we incorporated a CW 532 nm laser, what provides possibility of RRS measurements. For the first time, we demonstrate RRS measurements together with CRS and RRS performed on the same microscope on the example of cytochromes in the mitochondria of live leukemic cells (**Fig. 3**)[19]. SRS images (

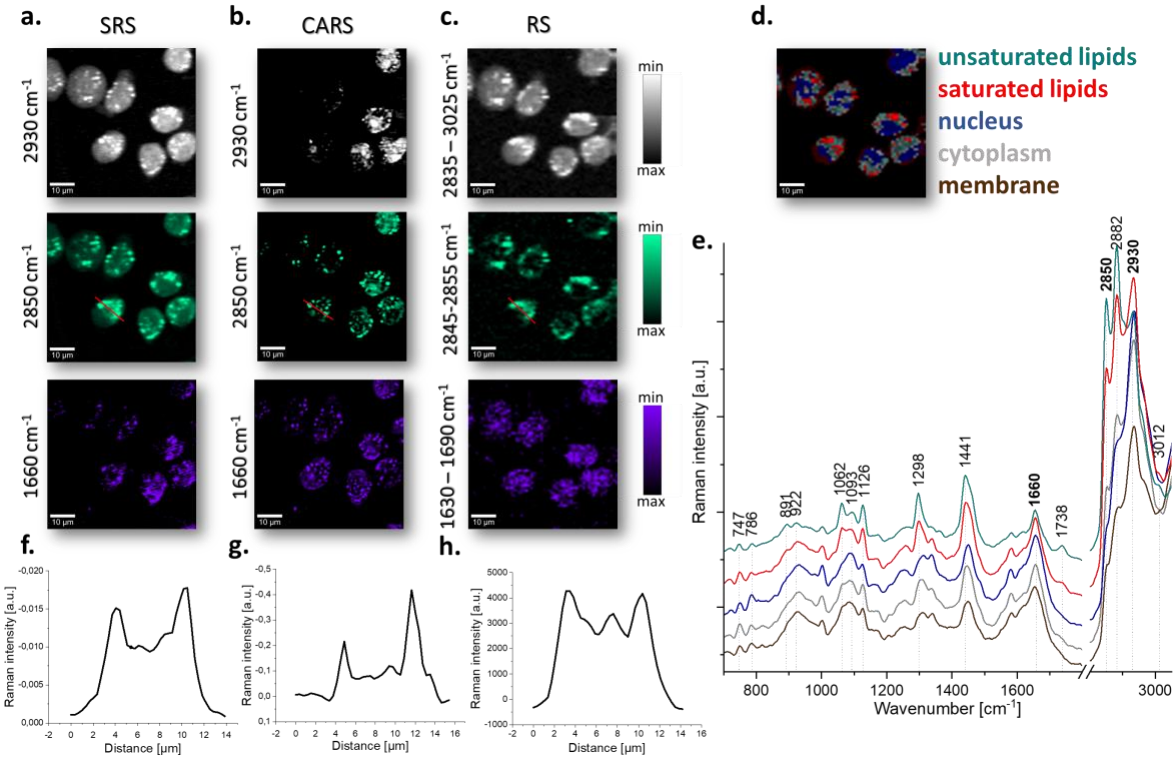

***Fig. 3*3a**) were collected using a pump beam at 879 nm (1660 cm^{-1}), corresponding to lipids and proteins and showing cell morphology, and 884 nm (1590 cm^{-1}), mainly corresponding to cytochromes c and b[20]. RS images of representative cells (

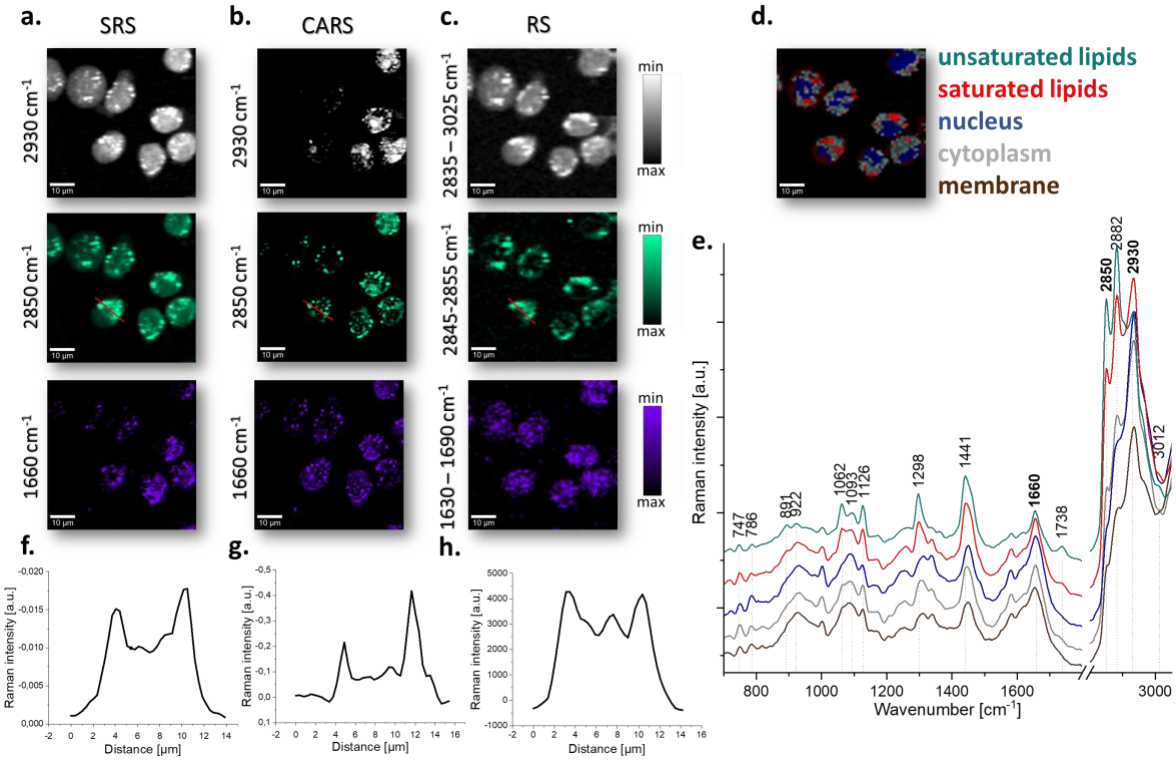

*Fig. 3*3**b**) were obtained by integrating the characteristic Raman bands, providing information on lipids and proteins (1630-1690 cm^{-1}, v(C=C) stretching, amide I) and the subcellular location of heme proteins (1573-1593 cm^{-1}, v($C_{\alpha}C_{m}$) stretching of the heme group)[21]. Using KMC analysis, it was possible to show the spatial distribution of the subcellular components (

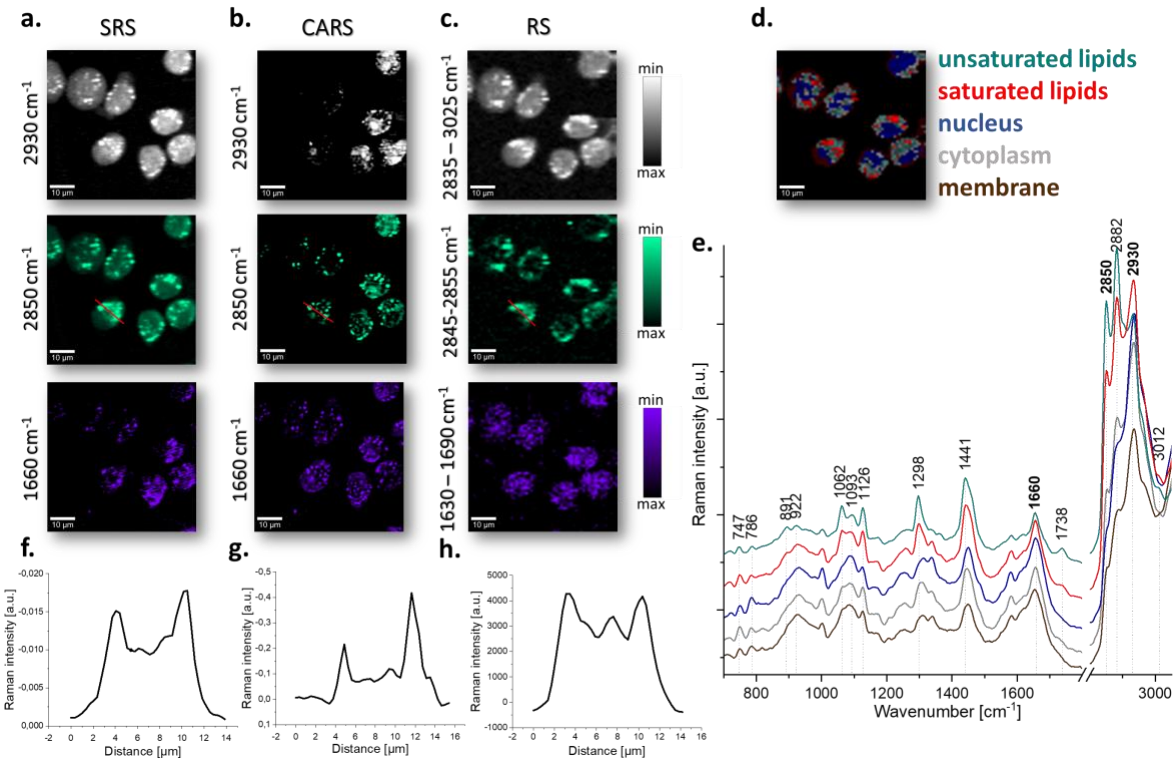

*Fig. 3*3**c**), including mitochondria. The mean spectra of mitochondria, lipids, nucleus, cytoplasm, and membrane are presented in **Fig. 3d**. As one can see, the Raman spectrum of

mitochondria is intense, and thanks to RRS, the specific bands for the cytochromes are well resolved (752, 1128, 1312, 1583 cm^{-1})[20,22,23]. Furthermore, the distribution of cytochromes obtained by RRS imaging can be easily tracked using the 1590 cm^{-1} band (**Fig. 3b**), which was confirmed by KMC analysis (**Fig. 3c**). On the contrary, the SRS image at 1590 cm^{-1} (**Fig. 3a**) does not show the distribution of mitochondria so clearly as the RRS image. To avoid photodamage and reduce the RRS signal from cytochromes, SRS and RS imaging were performed on different sets of cells. As seen in this example, TRAM enables the use of RRS imaging, which allows the unique use of the resonance phenomenon to enhance the Raman signal of specific groups of molecules.

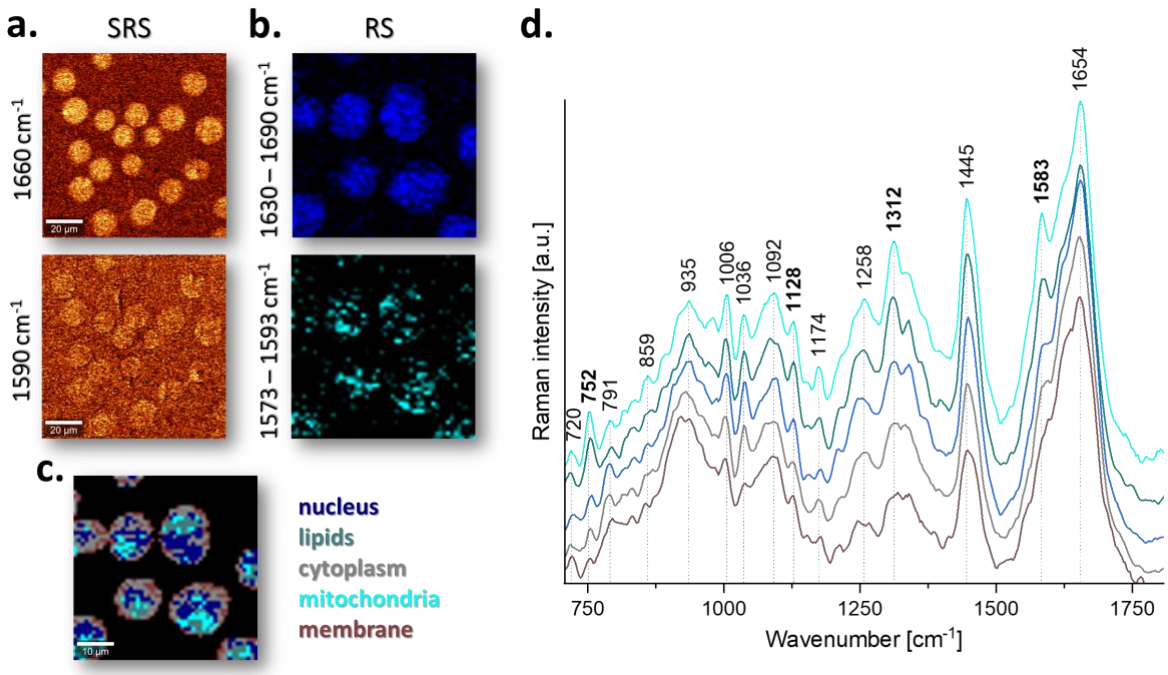

***Fig. 4. SRS/RS images of live HL-60 cells**. **a**. SRS images were collected using a pump beam of 879 nm (1660 cm^{-1}, lipids and proteins), and 884 nm (1590 cm^{-1}, mainly cytochromes in mitochondria), respectively. b. Representative RS images were obtained by the integration of the selected Raman bands at 1630-1690 cm^{-1} (lipids and proteins), and 1573-1593cm^{-1} (mainly cytochromes in mitochondria, exhibiting RRS), respectively. **c**. KMC map, showing the distribution of cell components in HL-60 cells. **d.** The averaged Raman spectra of cell components: lipids (green), mitochondria (light blue), nucleus (blue), cytoplasm (grey), and membrane (brown). Scale bar: 10µm. SRS and RS scans were performed using a galvo-scanner.*

TRAM in material science

To present the versatility of our setup, additionally, the measurements of PS beads were done. **Fig. 4a-c** presents SRS, CARS and, RS images of PS beads. The SRS and CARS images (**Fig. 4a-b**) were collected using a pump beam at 783 nm (3055 cm^{-1}) corresponding to aliphatic and aromatic C–H stretch vibration of PS, 792 nm (2905 cm^{-1}) corresponding to C−H stretch vibration of PS, and 883 nm (1604 cm^{-1}) corresponding to aromatic C−C stretch vibration of PS. RS images (**Fig. 4c**) were obtained by integrating the characteristic Raman bands at 3055 cm^{-1}, 2905 cm^{-1}, and 1604 cm^{-1}. In **Fig. 4e the** Raman spectrum of polystyrene is presented to visualize the differences in the intensity of Raman bands.

In **Fig. 4f-h**, the signal-to-noise ratio calculated along the cross-section in images showing the distribution of the 3055 cm^{-1} band is presented. In the case of CRS, this ratio is about six and ten times higher, respectively, for CARS (101.89) and SRS (59.43) images in comparison to the corresponding RS (10.84) image. SRS signal does not suffer from a non-resonant

background, which highly improves the quality of SRS maps, and lowers the noise. However, for the 2905 cm^{-1} band, the weaker CARS signal appears to be excessively faint, suggesting potential additional effects imposed on CARS observation. Conversely, for the 1604 cm^{-1} band, the CARS signal seems to be significantly stronger than expected, surpassing even the SRS signal strength, indicative of potential additional non-resonant background.

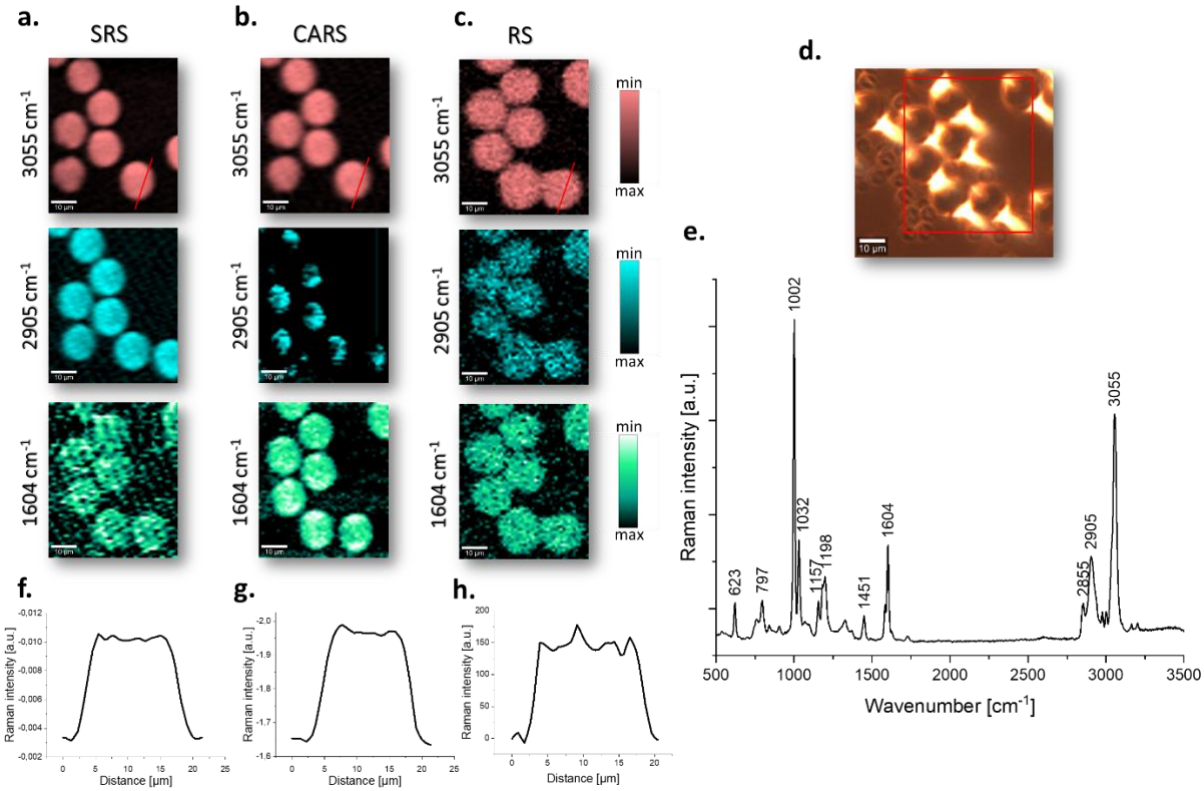

Fig. 4s. SRS/CARS/RS images of PS beads. a. – b. *SRS and CARS images were collected using a pump beam of 783 nm (3055 cm^{-1}), 792 nm (2905 cm^{-1}), and 883 nm (1604 cm^{-1}), respectively.* ***c****. Representative RS images were obtained by the integration of the selected Raman bands at 3055 cm^{-1}, 2905 cm^{-1}, and 1604 cm^{-1} respectively.* ***d****. Bright field of the measured field.* ***e.*** *The averaged Raman spectra of PS beads.* ***f-h****. Intensity profiles of Raman signal collected along the cross-section (highlighted in red) using SRS, CARS, and RS, respectively. Scale bar: 10µm. SRS and RS scans were performed respectively using a galvo-scanner and a translation table.*

Discussion

The integration of RS, CARS, and SRS into a single multimodal microscope represents a significant step forward in the field of spectroscopy and microscopy. This innovative combination harnesses the strengths of these techniques, offering a comprehensive tool for the detailed analysis, especially of biological samples, including live cells. Furthermore, this multimodal approach allows for the simultaneous collection of both broad spectral information and the targeted analysis of specific Raman bands.

To sum up, the advantages and implications of TRAM are the following.

1. Uniqueness and innovation: Simultaneous usage of both (R)RS and CRS techniques in a single device is a novel method. While each technique offers valuable insights, its combination as a single microscope amplifies its advantages. This unique combination ensures a comprehensive Raman spectrum to be obtained using RS and then a rapid image of specific components is taken using the CRS techniques. Furthermore, the ability to scan samples using two scanning techniques, i.e. a piezo-driven stage and galvo mirrors, significantly enhances the

versatility and efficiency of the system. The use of the piezo stage for scanning in RS measurements allows for a thorough analysis of large sample areas, which is crucial to obtain representative and comprehensive spectroscopic results. On the other hand, employing galvo mirrors in the CRS techniques enables much faster imaging of specific molecular components, i.e. while the piezo stage allows for achieving PDT of the order of ms, the galvo scanner allows for PDT of μs. TRAM is particularly useful in studies requiring high resolution and speed, such as real-time imaging of dynamic biological processes. Combining both scanning techniques in one device opens new possibilities for investigating the structure and dynamics of complex samples while significantly reducing the time needed to conduct experiments. This innovative configuration not only facilitates more accurate investigations but also contributes to the development of more advanced spectroscopic analytic methods.

The ability to quickly scan the RS excitation beam is particularly useful for samples with a large Raman cross-section. TRAM may change the perception of RS microscopy as a relatively slow method.

2. Consistency in measurements: One of the advantages of this integrated approach is the ability to multimodal measurement of the same sample under the same conditions. This is particularly important for non-adhesive cells, such as suspension cells not attached to a dish. The system enables direct data integration by correlating RS, SRS and CARS signals at the single pixel level. Furthermore, the act of immersing an objective lens into the sample itself can disturb the cells, causing them to move. A major benefit of a tandem system is that once the sample is placed, it can be measured using different techniques without any displacement, ensuring that the area under investigation is not lost. This capability is invaluable, particularly for studies involving sensitive or dynamic cellular processes, as it allows uninterrupted, consistent observation, and further comprehensive analysis, including data fusion. By minimizing the handling of the sample and reducing exposure to potentially harmful conditions, the accuracy and reliability of the collected data are maintained

3. Enhanced efficiency: The integration of CRS and (R)RS techniques into a single device significantly increases the efficiency of the analysis. The speed of the CRS techniques, which allows for ultra-fast high-quality imaging and molecular characterization perfectly complements the RS method providing full spectral information. This complementarity enables the comprehensive utilization of both techniques within one microscope, not only shortening the time required to perform CRS and RS measurements but also increasing the precision and reliability of the collected data. Through this combination, it is possible to move quickly from observing the general structures of a sample to in-depth molecular analysis without losing time for sample repositioning and recalibration.

4. **Further upgrade:** TRAM offers the potential for expansion to include additional imaging techniques such as, for example, the second harmonic generation (SHG) technique. By employing appropriate filters, dichroic mirrors, and additional detection, it is possible to split the signal for simultaneous detection of CARS, SRS, and SHG signals. Such an integration would allow concurrent imaging of multiple properties of samples with unprecedented accuracy and detail. While incorporation of CARS provides vibrational contrast, adding another layer of information to the images generated by SRS, the SHG utilizing the generation of the second harmonic, would enable the observation of structures like collagen or muscle fibers with unique contrast [38,39]. The separation of signals and simultaneous detection of these signals open new avenues in the structural and functional studies of various cell types and tissues, offering a comprehensive insight into their complex interactions and dynamics.

Even though it is not yet cost-effective and portable, our integrated system represents a significant step toward developing a method that enables comprehensive observation of Raman phenomena across diverse physical origins, encompassing both linear and nonlinear effects. Hence, our approach may promote the perception of Raman spectroscopy as a standalone

technique, obviating the need for reference techniques in advanced optical imaging, while ensuring complex sample characterization.

Conclusions

TRAM, combing CARS, SRS, and (R)RS together within one microscope is a significant step forward in the field of spectroscopy and microscopy. This opens up new opportunities in research and facilitates sample analysis while setting a new high standard in this field. The prospects for the development and application of this technology are enormous and diverse. The unique capabilities of the device can be further improved and developed. It can be integrated with additional imaging techniques, e.g. SHG, and fluorescence microscopy, to provide a more comprehensive sample analysis. In terms of applications, TRAM opens up new possibilities for research in biology, chemistry, medicine, and materials science.
Despite these innovations, there are still challenges associated with the sensitivity and specificity of Raman microscopy. However, the integration of CARS, SRS and, (R)RS within a single microscope facilitates addressing these issues, enabling more effective and precise adjustments. As a result, the parameters of the measurement can be better controlled, compared, and optimized, helping to further improve the sensitivity and specificity of spectral imaging.

Acknowledgment

This research was funded in whole or in part by the National Science Center Poland (NCN), Maestro 2022/46/A/ST4/00054 to Malgorzata Baranska. For Open Access, the author has applied a CC-BY public copyright license to any Author Accepted Manuscript (AAM) version arising from this submission.

References

1. Raman, C. V & Krishnan, K. S. The Optical Analogue of the Compton Effect. *Nature* **121**, 711 (1928).

2. Deng, C., Brooks, S. D., Vidaurre, G. & Thornton, D. C. O. Using Raman Microspectroscopy to Determine Chemical Composition and Mixing State of Airborne Marine Aerosols over the Pacific Ocean. *Aerosol Science and Technology* **48**, 193–206 (2014).

3. Cheng, Q., Miao, Y., Wild, J., Min, W. & Yang, Y. Emerging applications of stimulated Raman scattering microscopy in materials science. *Matter* **4**, 1460–1483 (2021).

4. Palonpon, A. F., Sodeoka, M. & Fujita, K. Molecular imaging of live cells by Raman microscopy. *Curr Opin Chem Biol* **17**, 708–715 (2013).

5. Carlomagno, C. *et al.* Human salivary Raman fingerprint as a biomarker for the diagnosis of Amyotrophic Lateral Sclerosis. *Sci Rep* **10**, 10175 (2020).

6. Katharina Eberhardt Clara Stiebing, C. M. M. S. & Popp, J. Advantages and limitations of Raman spectroscopy for molecular diagnostics: an update. *Expert Rev Mol Diagn* **15**, 773–787 (2015).

7. Min, Y.-K., Yamamoto, T., Kohda, E., Ito, T. & Hamaguchi, H. 1064 nm near-infrared multichannel Raman spectroscopy of fresh human lung tissues. *Journal of Raman Spectroscopy* **36**, 73–76 (2005).

8. Pezacki, J. P. *et al.* Chemical contrast for imaging living systems: molecular vibrations drive CARS microscopy. *Nat Chem Biol* **7**, 137–145 (2011).

9. Freudiger, C. W. *et al.* Stimulated Raman scattering microscopy with a robust fibre laser source. *Nat Photonics* **8**, 153–159 (2014).

10. Begley, R. F., Harvey, A. B. & Byer, R. L. Coherent anti-Stokes Raman spectroscopy. *Appl Phys Lett* **25**, 387–390 (1974).

11. Yamato, N., Niioka, H., Miyake, J. & Hashimoto, M. Improvement of nerve imaging speed with coherent anti-Stokes Raman scattering rigid endoscope using deep-learning noise reduction. *Sci Rep* **10**, 15212 (2020).

12. Li, S., Li, Y., Yi, R., Liu, L. & Qu, J. Coherent Anti-Stokes Raman Scattering Microscopy and Its Applications. *Front Phys* **8**, (2020).

13. Zhang, D., Wang, P., Slipchenko, M. N. & Cheng, J.-X. Fast vibrational imaging of single cells and tissues by stimulated Raman scattering microscopy. *Acc Chem Res* **47**, 2282–2290 (2014).

14. Li, Y. *et al.* Review of Stimulated Raman Scattering Microscopy Techniques and Applications in the Biosciences. *Adv Biol* **5**, 2000184 (2021).

15. Cheng, J.-X. & Xie, X. S. Vibrational spectroscopic imaging of living systems: An emerging platform for biology and medicine. *Science (1979)* **350**, aaa8870 (2015).

16. De La Cadena, A. *et al.* Broadband-stimulated Raman imaging based on multi-channel lock-in detection for spectral histopathology. *APL Photonics* **7**, (2022).

17. Klossek, A. *et al.* Studies for improved understanding of lipid distributions in human skin by combining stimulated and spontaneous Raman microscopy. *European Journal of Pharmaceutics and Biopharmaceutics* **116**, 76–84 (2017).

18. Slipchenko, M. N. *et al.* Vibrational imaging of tablets by epi-detected stimulated Raman scattering microscopy. *Analyst* **135**, 2613–2619 (2010).

19. Tipping, W. J., Lee, M., Serrels, A., Brunton, V. G. & Hulme, A. N. Stimulated Raman scattering microscopy: an emerging tool for drug discovery. *Chem. Soc. Rev.* **45**, 2075–2089 (2016).

20. Stiebing, C. *et al.* Real-time Raman and SRS imaging of living human macrophages reveal cell-to-cell heterogeneity and dynamics of lipid uptake. *J Biophotonics* **10**, 1217–1226 (2017).

21. Li, J. & Cheng, J. X. Direct visualization of de novo lipogenesis in single living cells. *Sci Rep* **4**, (2014).

22. Wang, S. *et al.* An insight into liquid water networks through hydrogen bonding halide anion: Stimulated Raman scattering. *J Appl Phys* **119**, (2016).

23. Li, H. *et al.* Imaging Chemical Kinetics of Radical Polymerization with an Ultrafast Coherent Raman Microscope. *Advanced Science* **7**, (2020).

24. Nan, X., Cheng, J.-X. & Xie, X. S. Vibrational imaging of lipid droplets in live fibroblast cells with coherent anti-Stokes Raman scattering microscopy. *J Lipid Res* **44**, 2202–2208 (2003).

25. Wang, H., Fu, Y., Zickmund, P., Shi, R. & Cheng, J.-X. Coherent Anti-Stokes Raman Scattering Imaging of Axonal Myelin in Live Spinal Tissues. *Biophys J* **89**, 581–591 (2005).

26. Le, T. T., Duren, H. M., Slipchenko, M. N., Hu, C.-D. & Cheng, J.-X. Label-free quantitative analysis of lipid metabolism in living Caenorhabditis elegans. *J Lipid Res* **51**, 672–677 (2010).

27. Slipchenko, M. N., Le, T. T., Chen, H. & Cheng, J.-X. High-Speed Vibrational Imaging and Spectral Analysis of Lipid Bodies by Compound Raman Microscopy. *J Phys Chem B* **113**, 7681–7686 (2009).

28. Adams, W. R. *et al.* Multi-modal nonlinear optical and thermal imaging platform for label-free characterization of biological tissue. *Sci Rep* **11**, 8067 (2021).

29. Crisafi, F. *et al.* Multimodal nonlinear microscope based on a compact fiber-format laser source. *Spectrochim Acta A Mol Biomol Spectrosc* **188**, 135–140 (2018).

30. Aird, W. C. Phenotypic heterogeneity of the endothelium: I. Structure, function, and mechanisms. *Circ Res* **100**, 158–173 (2007).

31. Galley, H. F. & Webster, N. R. Physiology of the endothelium. *Br J Anaesth* **93**, 105–113 (2004).

32. Collins, S. J. The HL-60 promyelocytic leukemia cell line: proliferation, differentiation, and cellular oncogene expression. *Blood* **70**, 1233–1244 (1988).

33. Birnie, G. D. The HL60 cell line: A model system for studying human myeloid cell differentiation. *Br J Cancer* **58**, 41–45 (1988).

34. Radwan, B. *et al.* EdU sensing: The Raman way of following endothelial cell proliferation in vitro and ex vivo. *Biosens Bioelectron* **216**, 114624 (2022).

35. Bulat, K., Rygula, A., Szafraniec, E., Ozaki, Y. & Baranska, M. Live endothelial cells imaged by Scanning Near-field Optical Microscopy (SNOM): capabilities and challenges. *J Biophotonics* **10**, 928–938 (2017).

36. Majzner, K. *et al.* 3D confocal Raman imaging of endothelial cells and vascular wall: perspectives in analytical spectroscopy of biomedical research. *Analyst* **138**, 603–610 (2013).

37. Terhune, R. W., Maker, P. D. & Savage, C. M. Measurements of nonlinear light scattering. *Phys Rev Lett* **14**, 681 (1965).

38. Both, M. *et al.* Second harmonic imaging of intrinsic signals in muscle fibers *in situ*. *J Biomed Opt* **9**, 882–892 (2004).

39. Chen, X., Nadiarynkh, O., Plotnikov, S. & Campagnola, P. J. Second harmonic generation microscopy for quantitative analysis of collagen fibrillar structure. *Nat Protoc* **7**, 654–669 (2012).